J Mater Sci (2010) 45:1528–1539
DOI 10.1007/s10853-009-4118-z

Effects of Mg, Fe, Be additions and solution heat treatment on the π-AlMgFeSi iron intermetallic phase in Al–7Si–Mg alloys

E. A. Elsharkawi · E. Samuel · A. M. Samuel · F. H. Samuel

Received: 4 September 2009 / Accepted: 7 December 2009 / Published online: 5 January 2010

Abstract The presence of magnesium in Be-free Al–7Si–Mg alloys results in the formation of an undesirable iron-intermetallic known as the π-AlMgFeSi phase. The effect of Mg, Fe, and Be on the formation of this phase in both unmodified and Sr-modified Al–7Si–*x*Mg–*y*Fe alloys containing 0.4–0.8-wt% Mg and 0.1–0.8-wt% Fe has been investigated at a dendrite arm spacing of 65 μm. A qualitative microstructural examination was carried out to study the effect of solution heat treatment (540 °C/8 h) on the decomposition of the π-AlMgFeSi phase ("π-phase") in Al–7Si–*x*Mg–0.1Fe alloys containing 0.4–1.0-wt% Mg. The results indicate that increasing the Mg and Fe content increases the amount of the π-AlMgFeSi phase formed. Quantitative measurements revealed a reduction in the surface fraction of the π-phase after solution heat treatment. Different levels of decomposition of the π-phase into needles of β-Al_5FeSi iron intermetallic phase ("β-phase") were observed at 0.4-, 0.6-, and 0.8-wt% Mg, after solution heat treatment.

Introduction

Aluminum alloys are vital in various industrial applications, owing to a combination of favorable physical and mechanical properties. The addition of silicon results in high fluidity, good feedability characteristics, low shrinkage, and satisfactory crack resistance. The further addition of magnesium results in a family of Al–Si–Mg alloys, such as the 356 and 357 Al–7%Si–Mg alloys, which have been used extensively in automotive and aerospace applications [1–3]. When iron is added to Al–7%Si–Mg alloys, it forms a platelet-like β-Al_5FeSi iron-intermetallic phase ("β-phase") with sharp edges. The high stress concentrations at these sharp edges [4], as well as the weak bonding between the β-phase and the Al matrix [5], enhance crack initiation and, thus decrease the ductility of the castings. In the case where Mg is present, the π-AlFeMgSi iron-intermetallic phase ("π-phase") forms, displaying a script-like morphology with a stoichiometry close to $Al_8FeMg_3Si_6$ [6].

The formation of the π-phase in Al–7Si–Mg alloys [6] occurs via two reported reactions: (1) as a result of the transformation of the β-phase into the π-phase through a peritectic reaction ($L + Al_5FeSi \rightarrow Al + Si + Al_8Mg_3FeSi_6$), or, (2) as a result of the quaternary eutectic reaction at the end of the solidification sequences ($L \rightarrow Al + Si + Mg_2Si + Al_8Mg_3FeSi_6$). It has been observed that the Fe-rich intermetallic phases in the Al–7Si–Mg alloy with 0.4-wt% Mg were exclusively small β-phase plates, while large π-phase particles were dominant in the high Mg-containing alloys with a small proportion of the β-phase [7]. Wang [8] reported that increasing the Mg content in 357 alloys significantly increases the potential for the formation of the Mg-containing iron intermetallic $Al_8Mg_3FeSi_6$ phase.

Magnesium is added to Al–7Si–Mg alloys to promote the formation of the Mg_2Si phase which precipitates during aging, hardens the alloy and, consequently, improves the yield strength and ductility [9, 10]. The ultimate tensile strength (UTS) and yield strength (YS) values will gradually level off at high Mg levels, while ductility decreases [11, 12]. Cáceres et al. [7] attributed this reduction to the presence of the π-phase which is larger than the Si particles in Sr-modified 357 alloys. Likewise, the fracture of the

E. A. Elsharkawi · E. Samuel · A. M. Samuel · F. H. Samuel (✉)
Département des Sciences Appliquées, Université du Québec à Chicoutimi, Chicoutimi, QC G7H 2B1, Canada
e-mail: fhsamuel@uqac.ca

π-phase particles further was observed to lower ductility, especially in Sr-modified 357 alloys [8].

Formation of the π-phase consumes large amounts of Mg from the solution during solidification, thereby reducing the amount of free Mg available to form Mg_2Si precipitates during aging, leading to the saturation of the UTS and YS [13, 14]. Beryllium behaves as a neutralizing agent for the Fe intermetallic phases which form in Al–7Si–Mg alloys, where the formation of the π-phase is suppressed by the addition of Be to 357 alloys [14]. The presence of Be in premium quality aluminum alloys leads to the production of a clean melt and to the formation of an oxidation layer which prevents Mg from oxidizing [15], hence increasing the amount of free Mg available to form Mg_2Si for strengthening.

An addition of 0.05-wt% Be in A357 alloy was reported to result in the replacement of the β-phase into α-Al_8Fe_2Si with a script morphology, thereby reducing the angularity effect of the β-phase, and thus improving strength and ductility [16]. Others have shown that the addition of Be to an Al–7Si–0.3Mg alloy alters the composition and morphology of the β-phase into a Chinese-script Be–Fe phase [17, 18]. On the other hand, the presence of Be in A357 alloys is a potential health hazard and its elimination is highly recommended [15]. Experiments demonstrating the possibility of eliminating Be from this alloy without any loss to mechanical properties have shown that this is only feasible if the iron content is reduced [14].

A typical ASM standard heat treatment consists of (i) solid solution treatment, (ii) quenching, and (iii) a combination of natural and artificial aging. The heat treatment of Al–7Si–Mg alloys is carried out to obtain the best combination of strength and ductility. Solution heat treatment results in the dissolution of Mg_2Si particles, the homogenization of the casting and a transformation in the morphology of eutectic silicon by fragmentation and spheroidization as well as the dissolution or transformation of iron-rich intermetallic phases [19–21]. Closset and Gruzleski [22] observed that the π-phase in solution heat-treated 356 alloys dissolves at 0.16-wt% Fe and 0.45-wt% Mg, whereas it is only partially dissolved at higher 0.65-wt% Mg. Gustafsson et al. [23]. noted that the π-phase in 356 alloys only dissolved after solution heat treatment, although no changes were observed in the β-phase.

In a recent study by Taylor et al. [24], the authors reported that the as-cast Chinese-script π-phase in Al–7Si–*x*Mg alloys containing 0.12-wt% Fe and low levels of Mg (0.3–0.4 wt%) reduced in amount as a result of a transformation into clusters of fine β-phase needles. At an intermediate Mg level (0.5 wt%), there is a partial transformation of π-phase into β-phase needles, whereas no change is observed at higher Mg levels (~0.6–0.7 wt%). Wang and Davidson [13] also reported that at Mg levels of 0.4 wt%, the π-phase in Al–7Si–Mg alloys decomposed into fine β-phase platelets as a result of the release of Mg into the matrix. However, at >0.4-wt% Mg, the π-phase has a tendency to become slightly spheroidized. This may be attributed to the solubility limit of Mg in the Al matrix.

The aim of this study is to attain an understanding of the role of Fe, Mg, Sr, and Be as well as the interaction between them in the formation of the π-phase iron-intermetallic in the as-cast and solution heat-treated conditions in Al–7Si–*x*Mg–*y*Fe alloys.

Experimental procedures

Alloys preparation and casting

The chemical composition of the as-received 356 alloy is given in Table 1. Melting was carried out in a SiC crucible of a 25-kg capacity using an electrical resistance furnace and the melting temperature was maintained at 740 ± 5 °C. Silicon and magnesium were added in their pure form, while iron and beryllium were added in the form of Al–25%Fe and Al–5%Be master alloys, respectively. A combination of Ti and B was added to the melt in the form of Al–5%Ti–1%B master alloy rods for the purposes of grain refinement. The Sr-modified alloys were obtained by the addition of 200-ppm Sr in the form of an Al–10%Sr master alloy to the as-received alloys to modify the eutectic silicon particles from acicular into fibrous shape [25].

The melts were subsequently degassed and stirred for 10 min. The degassing process was carried out using pure dry argon injected into the molten metal at a constant rate of 30 ft^3/h by means of a rotary graphite impeller. Following this, the melt was carefully skimmed to remove oxide layers from the surface of the melt. Finally, the molten metal for each composition was then poured into a cylindrical graphite mold 80 mm in height, 60 mm in diameter, and preheated to 600 °C so as to create a slow cooling rate resembling equilibrium conditions. Samples were simultaneously taken from each melt condition for chemical analysis. The chemical compositions of the prepared 356 and 357 alloys used for quantitative and qualitative analyses are listed in Tables 2 and 3, respectively.

A high sensitivity type-K thermocouple was attached along the center-line of the mold cavity to the center of the graphite mold. The portion of the thermocouple within the

Table 1 Chemical composition of the as-received 356 alloy

Alloy	Element (wt%)							
	Si	Fe	Mg	Mn	Cu	Ti	Sr	Al
356	7.32	0.09	0.38	<0.01	0.1	0.12	0.002	Bal.

Table 2 Chemical composition of 356 and 357 alloys

	Element (wt%)							
	Si	Fe	Mg	Mn	Cu	Ti	Sr	Al
356 alloy codes								
1[a]	7.22	0.10	0.42	0.00	0.02	0.12	0.00	Bal.
2	7.04	0.25	0.41	0.02	0.10	0.11	0.00	Bal.
3	7.16	0.46	0.41	0.03	0.11	0.09	0.00	Bal.
4	6.90	0.64	0.41	0.02	0.11	0.11	0.00	Bal.
5	7.09	0.83	0.39	0.03	0.11	0.16	0.00	Bal.
1S[a]	7.13	0.10	0.41	0.01	0.02	0.11	0.02	Bal.
2S	6.72	0.24	0.46	0.02	0.11	0.11	0.02	Bal.
3S	7.02	0.43	0.46	0.03	0.11	0.10	0.02	Bal.
4S[a]	6.77	0.55	0.43	0.03	0.10	0.10	0.02	Bal.
5S	7.00	0.80	0.37	0.0	0.04	0.10	0.02	Bal.
357 alloy codes								
6	7.00	0.10	0.60	0.00	0.01	0.10	0.00	Bal.
7	7.42	0.29	0.60	0.02	0.11	0.17	0.00	Bal.
8	7.17	0.44	0.60	0.02	0.11	0.14	0.00	Bal.
9	7.20	0.57	0.58	0.02	0.11	0.11	0.00	Bal.
10	7.41	0.75	0.59	0.03	0.11	0.19	0.00	Bal.
6S	7.00	0.10	0.56	0.02	0.10	0.10	0.02	Bal.
7S	7.00	0.26	0.60	0.02	0.10	0.10	0.02	Bal.
8S	7.00	0.40	0.60	0.02	0.10	0.10	0.02	Bal.
9S	7.00	0.60	0.53	0.02	0.10	0.10	0.02	Bal.
10S	7.00	0.78	0.65	0.02	0.10	0.10	0.02	Bal.
11[a]	7.18	0.10	0.75	0.02	0.10	0.13	0.00	Bal.
12	7.30	0.29	0.74	0.03	0.11	0.12	0.00	Bal.
13	7.31	0.38	0.76	0.03	0.11	0.16	0.00	Bal.
14	7.51	0.63	0.79	0.27	0.11	0.18	0.00	Bal.
15[a]	7.00	0.80	0.80	0.03	0.10	0.10	0.00	Bal.
11S	7.43	0.10	0.79	0.00	0.02	0.11	0.02	Bal.
12S	7.20	0.29	0.78	0.02	0.10	0.14	0.02	Bal.
13S	7.35	0.46	0.82	0.02	0.11	0.16	0.02	Bal.
14S[a]	7.44	0.55	0.78	0.03	0.11	0.14	0.02	Bal.
15S	7.75	0.80	0.72	0.03	0.11	0.10	0.02	Bal.
16[a]	7.47	0.10	1.00	0.00	0.02	0.10	0.00	Bal.
16S	7.16	0.10	1.00	0.00	0.00	0.10	0.02	Bal.

S Sr-modified

[a] Alloys used for qualitative analysis

mold was isolated using double-walled ceramic tube. From the thermal analysis data, the cooling curves and the corresponding first derivative curves were plotted to identify the main reactions and corresponding temperatures for the prepared alloys. Two 2.5 cm × 2.5 cm samples were sectioned off from each graphite mold casting, at the center of the casting near the thermocouple tip. A first set of samples was kept in the as-cast condition, while a second set was solution heat-treated (540 °C/8 h), followed by a warm water (60 °C) quench.

Table 3 Chemical composition of 356 and 357 alloys containing Be

	Element (wt%)								
	Si	Fe	Mn	Cu	Mg	Ti	Sr	Be	Al
356 alloy codes									
1B	7.06	0.11	0.02	0.20	0.36	0.10	0.003	0.055	Bal.
1BS	6.95	0.11	0.02	0.20	0.37	0.10	0.017	0.057	Bal.
357 alloy codes									
6B[a]	7.07	0.11	0.02	0.10	0.62	0.10	0.003	0.045	Bal.
6BS[a]	6.80	0.11	0.02	0.10	0.64	0.10	0.018	0.05	Bal.
16B[a]	6.63	0.11	0.02	0.16	1.00	0.10	0.003	0.05	Bal.
16BS[a]	7.12	0.11	0.02	0.06	1.00	0.10	0.023	0.06	Bal.

B Be-content, *S* Sr-modified

[a] Alloys used for qualitative analysis

Qualitative and quantitative microstructural analyses

The average dendrite arm spacing (DAS) was measured for the as-cast samples using a Clemex Vision PE 4.0 optical microscope equipped with an image analysis system. Thirty fields were used, covering the entire sample surface. Phase identification and quantitative surface fraction for the iron intermetallics were carried out for the as-cast and solution heat-treated conditions. Surface fraction of the π-phase iron intermetallic was quantified using a JEOL JXA-8900L model electron probe microanalyzer equipped with a special built-in software to calculate surface fraction of phases based on phase brightness. The brightness of each phase is a function of its average atomic number. The quantification process is based on the elimination technique by subtracting the surface fraction of the brighter phases from the total surface fraction of the phases present within the matrix. For each condition, 20 fields were examined at a magnification of ×100.

Results and discussion

Microstructural observations

The Al–7Si–*x*Mg–*y*Fe as-cast alloy microstructure (for 0.4-, 0.6-, and 0.8-wt% Mg and 0.1–0.8-wt% Fe), obtained from graphite mold castings (DAS = 65 μm) consists of primary α-Al dendrite, eutectic silicon, Mg_2Si, and iron intermetallics. The iron intermetallics observed are β-Al_5FeSi iron intermetallics with a platelet-like morphology and the π-AlFeMgSi iron intermetallic phase with a script-like morphology (Fig. 1). With regards to the π-phase, the suggestion of the stoichiometry by Foss et al. [26] was $Al_9FeMg_3Si_5$, which deviates from the previously suggested $Al_8FeMg_3Si_6$ [6, 22]. In this study, the calculated stoichiometry of the β- and π-phase iron intermetallics,

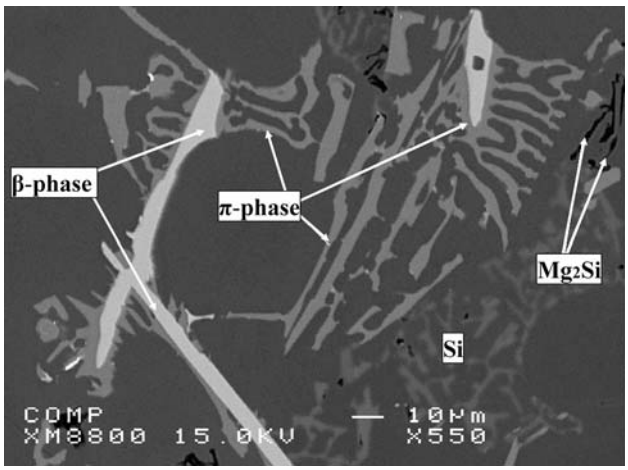

Fig. 1 Microstructure of the non-modified Al–7Si–0.8Mg–0.8Fe alloy (15)

based on the composition obtained using EPMA and WDS analyses in the as-cast condition in alloys 1 and 15, are in the vicinity of the suggested formulas [6], regardless of the Fe and Mg content of the alloy (Table 4).

Thermal analysis

Thermal analysis was carried out to determine the precipitation sequence and formation temperature of the iron intermetallics observed in alloys 1S (0.4%Mg–0.1%Fe) and 4S (0.4%Mg–0.55-wt% Fe). Based on the expected reactions [6], the reaction and corresponding temperatures obtained from the cooling curve for these alloys are listed in Table 5. As Fig. 2a reveals, solidification of the 1S alloy begins with the precipitation of α-aluminum (1), followed by formation of the Al–Si eutectic (2) along with the

Table 4 Chemical composition of the Fe intermetallic phases observed in this study

Alloy	Phase	Element				Formula	
		Al	Si	Fe	Mg	Calculated	Suggested [6, 22]
1 (356) 0.4Mg–0.1Fe	π	47.68	30.32	6.8	15.14	$Al_{9.4}Fe_{1.3}Mg_3Si_6$	$Al_8FeMg_3Si_6$
	β	63.00	20.91	16.2	0	$Al_{3.9}FeSi_{1.2}$	Al_5FeSi
15 (357) 0.8Mg–0.8Fe	π	47.85	26.86	6.03	19.07	$Al_{7.5}Fe_{0.94}Mg_3Si_{4.2}$	$Al_8FeMg_3Si_6$
	β	65.5	17.66	16.6	0	$Al_{3.9}FeSi_{1.06}$	Al_5FeSi

Table 5 Main reactions observed from thermal analysis data of alloys 1S, 4S, and 14S

Alloy codes	Temperature (°C)	Reactions [6]
1S(356): 0.1%Fe–0.4%Mg (Fig. 2)	611 (1)	Formation of Al-dendritic network
	570 (2)	Precipitation of eutectic silicon
		Precipitation of post-eutectic β-Al_5FeSi phase
	560 (3)	Transformation of β-phase into π-$Al_8Mg_3FeSi_6$ phase
	545 (4)	Precipitation of Mg_2Si
		Quaternary eutectic reaction[a]
4S(356): 0.55%Fe–0.4%Mg (Fig. 3)	611 (1)	Formation of Al-dendritic network
	577 (2)	Formation of pre-eutectic β-Al_5FeSi phase
	570 (3)	Precipitation of eutectic silicon
		Precipitation of post-eutectic β-Al_5FeSi phase
	553 (4)	Transformation of β-phase into π-$Al_8Mg_3FeSi_6$ phase
	543 (5)	Precipitation of Mg_2Si
		Quaternary eutectic reaction[a]
14S(357): 0.55%Fe–0.78%Mg (Fig. 4)	610 (1)	Formation of Al-dendritic network
	570 (2)	Formation of pre-eutectic β-Al_5FeSi phase
	560 (3)	Precipitation of eutectic silicon
		Precipitation of post-eutectic β-Al_5FeSi phase
	551 (4)	Transformation of β-phase into π-$Al_8Mg_3FeSi_6$ phase
		Precipitation of Mg_2Si
	539 (5)	Quaternary eutectic reaction[a]

[a] Quaternary eutectic reaction: $L \rightarrow Al + Si + Mg_2Si + Al_8Mg_3FeSi_6$

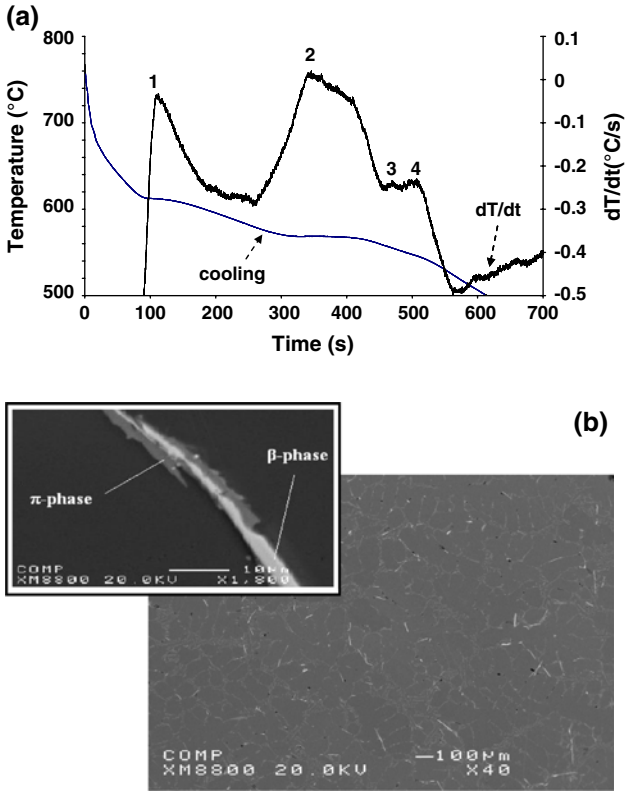

Fig. 2 **a** Temperature–time cooling curve and its first derivative obtained from the Sr-modified 356 alloy 1S and **b** the corresponding microstructure showing the small size of the β-phase and the π-phase particles

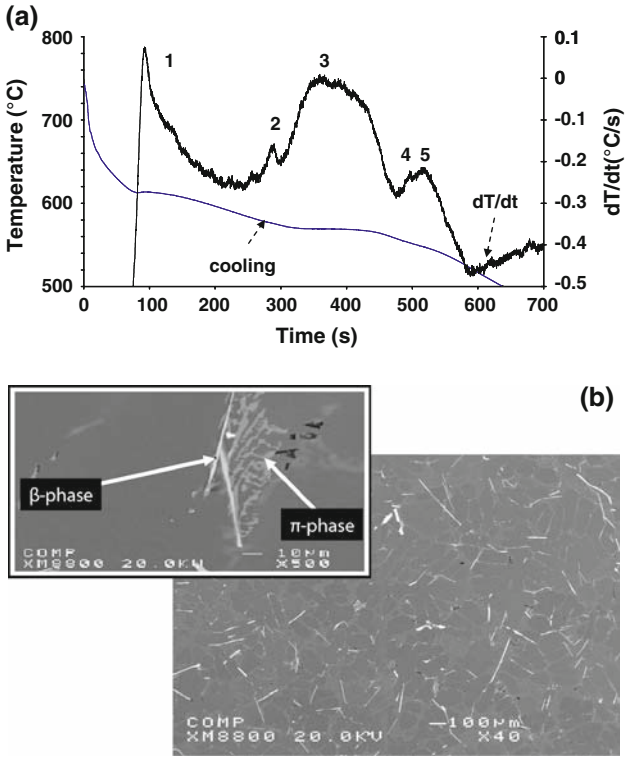

Fig. 3 **a** Temperature–time cooling curve and its first derivative obtained from the Sr-modified 356 alloy 4S and **b** the corresponding microstructure showing the large size of the β-phase and the π-phase particles

precipitation of the post-eutectic β-Al_5FeSi. It is expected that as solidification proceeds, the β-phase present will be transformed into the π-phase as a result of the peritectic reaction (3): ($L + Al_5FeSi \rightarrow Al + Si + Al_8Mg_3FeSi_6$). The last reaction to be detected is characterized by a wide peak, which may arise from two merged reactions (4). The first of these is related to the formation of Mg_2Si followed by the second reaction which corresponds to the quaternary eutectic reaction: ($L \rightarrow Al + Si + Mg_2Si + Al_8Mg_3FeSi_6$). Upon comparing the first-derivative curve in Fig. 2a with that in Fig. 3a for alloys 1S and 4S, respectively, it can be seen that at 0.1-wt% Fe (alloy 1S), the first-derivative curve reveals four peaks, while at 0.55-wt% Fe (alloy 4S), a new peak is detected before the eutectic silicon (marked as 2), corresponding to the formation of the pre-eutectic β-phase. Other reactions remain the same as described in Fig. 2.

It has been reported [27, 28] that increasing the Fe content from 0.1 to 0.55 wt% changes the solidification sequences of Al–7Si–0.4-Mg alloys; this is thoroughly supported by the current thermal analysis. At 0.1-wt% Fe, the β-phase precipitates at low temperatures together with the Al–Si eutectic and is characterized by fine platelets in the microstructure (Fig. 2b). However, at 0.54-wt% Fe, most of the β-phase will precipitate at high temperatures before the Al–Si eutectic. This β-phase is characterized by its large size in the microstructure (Fig. 3b). Consequently, increasing the Fe content will increase the quantity and size of the β-phase in the microstructure.

In order to arrive at a clearer understanding of the effect of magnesium in the precipitation sequence and reaction temperature, the Mg content in alloy 4S was increased to 0.8 wt% (alloy 14S). Two separate peaks were identified corresponding to reactions (4) and (5), as shown in Fig. 4. The reactions and corresponding temperature that occurs

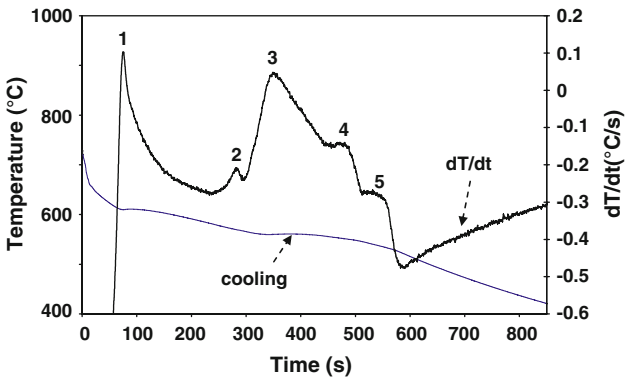

Fig. 4 Temperature-time cooling curve and its first derivative obtained from the Sr-modified 357 alloy 14S

during solidification of the alloys containing high (14S) and low Mg (4S) levels are listed in Table 5 for comparison purposes. There is a significant reduction in the eutectic temperature by ~10 °C in a higher Mg-containing alloy (14S) when compared to the low Mg-containing alloy (4S). This is in agreement with published findings [9, 29]. It has been reported that this reduction in eutectic temperature affects the eutectic Si particle modification [9, 29].

Upon examination of the microstructure, the π-$Al_8FeMg_3Si_6$ phase is often observed to be in close contact with β-Al_5FeSi phase platelets. It is revealed in the inset in Fig. 2b that the interface between the β- and π-phases is seamlessly fused together, which may lead to the assumption that the β-Al_5FeSi phase will precipitate as a first step, followed by the growth of the π-$Al_8FeMg_3Si_6$ phase from the surface of the β-Al_5FeSi phase as a second step, according to the peritectic reaction [6].

Quantitative analysis

Effects of Fe and Mg Content

Figure 5 illustrates the effects of Fe and Mg content on the surface fraction of the π-phase in non-modified and Sr-modified Al–7Si–*x*Mg–*y*Fe alloys in the as-cast and solution heat-treated conditions. As the Fe content is increased from 0.1 to 0.8 wt%, the π-phase surface fraction increases by varying degrees in the non-modified and Sr-modified alloys. Figure 5b demonstrates how the addition of 0.02-wt% Sr to Al–7Si–*x*Mg–*y*Fe alloys results in slight increases in the surface fraction of the π-phase when compared to Fig. 5a. This may be explained in terms of the presence of Sr which results in breaking up β-phase platelets [30], thereby reducing the length and increasing the density of β-phase platelets. The authors [30] claim that Sr was absorbed by β-phase platelets leading to their destabilization, and hence, fragmentation. This may contribute to an increase in the number of β-platelets available for the occurrence of the peritectic reaction to form more π-phase. It is apparent from Fig. 5 that the lowest amount of π-phase surface fraction at all Mg levels occurs at low Fe levels (0.1 wt%). Therefore, the use of primary Al–7Si–*x*Mg alloys containing low amounts of Fe is recommended from a practical viewpoint. In this study, a qualitative microstructural analysis will focus mainly on Al–7Si–*x*Mg–0.1Fe alloys.

Effect of solution heat treatment

Figure 5 also demonstrates the effect of solution heat treatment on the π-phase surface fraction in non-modified and Sr-modified Al–7Si–*x*Mg–*y*Fe alloys. In non-modified

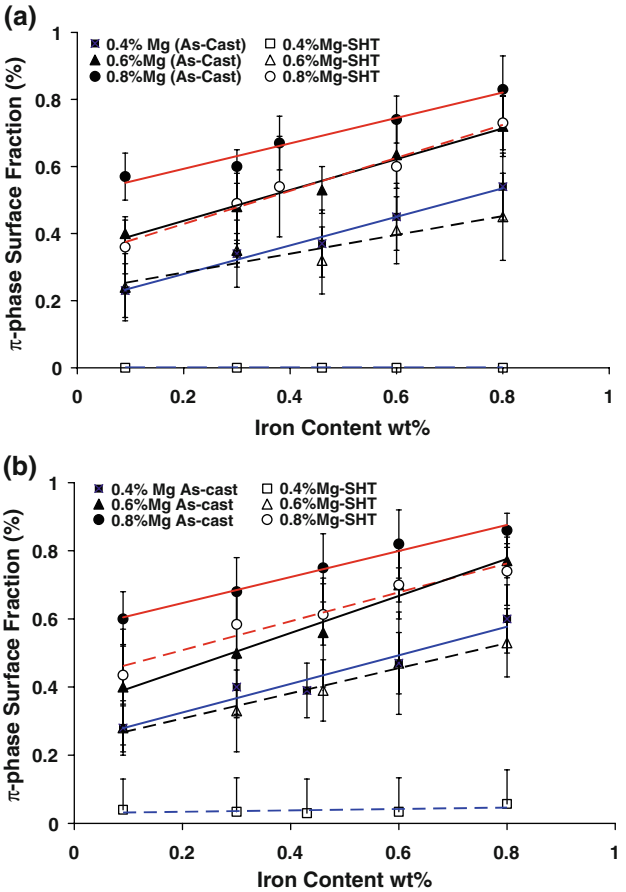

Fig. 5 Effects of Fe and Mg contents on the surface fraction of the π-phase intermetallic in Al–7Si–*x*Mg–*y*Fe alloys (DAS = 65 μm) in the as-cast and solution heat-treated (540 °C/8 h) conditions: **a** non-modified alloys and **b** Sr-modified alloys

Al–7Si–0.4Mg–*y*Fe alloys (Fig. 5a), the π-phase is almost completely dissolved at all Fe levels after solution heat treatment. The non-modified Al–7Si–0.4Mg–0.1Fe alloy microstructures shown in Fig. 6a and b support this observation. Figure 6a shows the π-phase in the as-cast condition, while Fig. 6b reveals the presence of fine needles in the microstructure after solution heat treatment. The X-ray images of the Fe and Mg distribution within these fine needles are presented in Fig. 6c and d, respectively, and support the claim that the fine needles are indeed β-phase needles. This suggests that, during solution heat treatment, the π-phase in the 356 alloy having 0.4-wt% Mg is completely decomposed into fine β-phase needles as a result of Mg which diffuses out from the π-phase and into the surrounding aluminum matrix. This observation confirms the findings of Taylor et al. [24] who reported that at 0.3–0.4-wt% Mg, the as-cast Chinese-script π-phase is reduced as a result of its transformation into clusters of fine β-phase needles.

On the other hand, in the solution heat-treated Sr-modified Al–7Si–0.4Mg–*y*Fe alloys, the π-phase is not

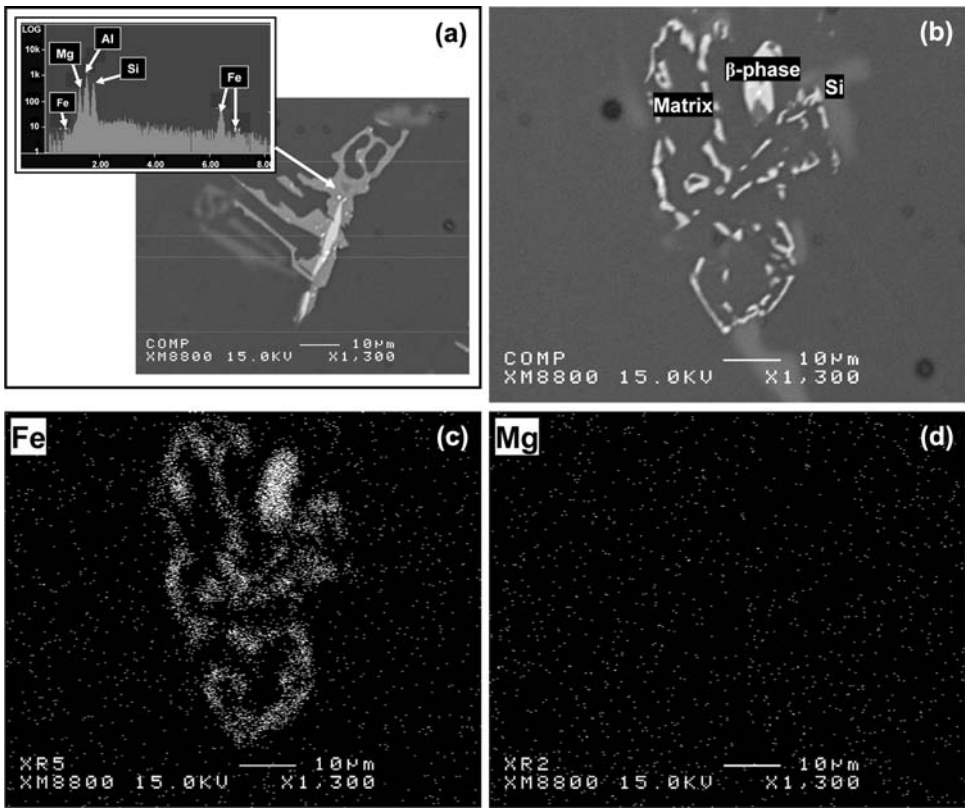

Fig. 6 **a**, **b** Backscattered electron images of non-modified 356 alloy coded 1 in the (**a**) as-cast condition, showing π- and β-phases, **b** after solution heat treatment (540 °C/8 h), showing complete decomposition of π-$Al_8Mg_3FeSi_6$ into fine β-Al_5FeSi needles, and X-ray images of Fe (**c**) and Mg (**d**) corresponding to (**b**)

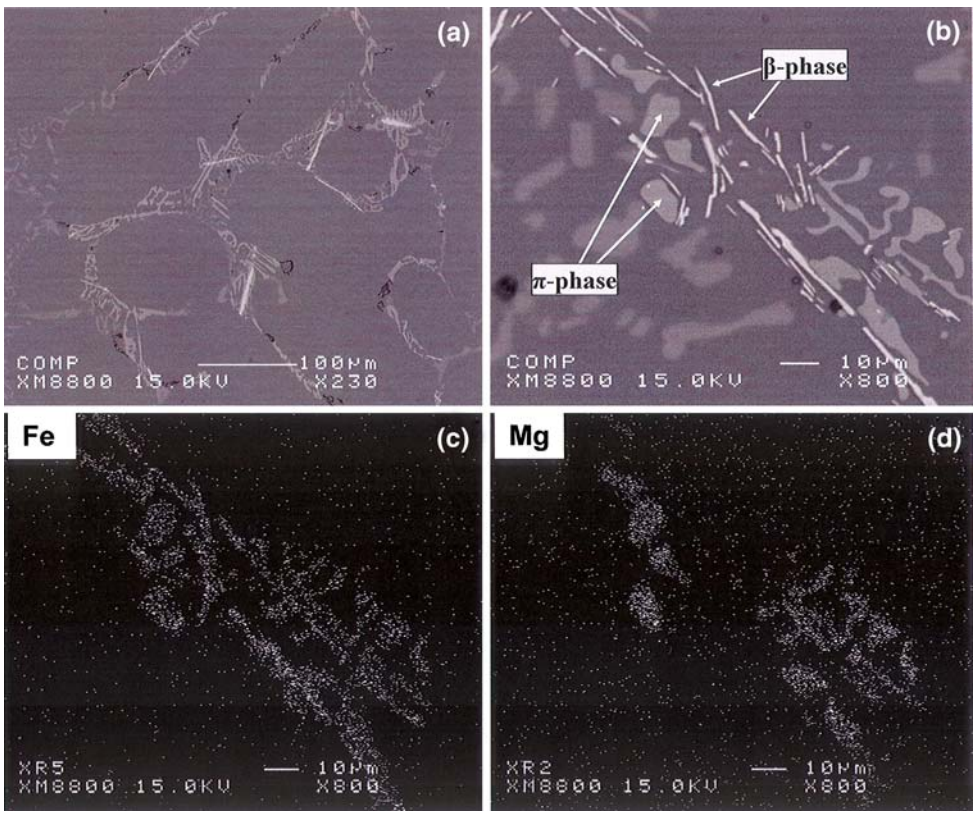

Fig. 7 **a**, **b** Backscattered electron images of Sr-modified 356 alloy coded 1S in the (**a**) as-cast condition, showing π- and β-phases, **b** after solution treatment (540 °C/8 h), showing partial decomposition of π-$Al_8Mg_3FeSi_6$ into fine β-Al_5FeSi needles, and X-ray images of Fe (**c**) and Mg (**d**) corresponding to (**b**)

completely decomposed after solution heat treatment (Fig. 5b). This observation is supported by the microstructures of the solution heat-treated Sr-modified Al–7Si–0.4Mg–0.1Fe alloy in Fig. 7a and b, where Fig. 7a shows the as-cast microstructure and Fig. 7b reveals fine needles accompanied by small spheroidized π-phase particles.

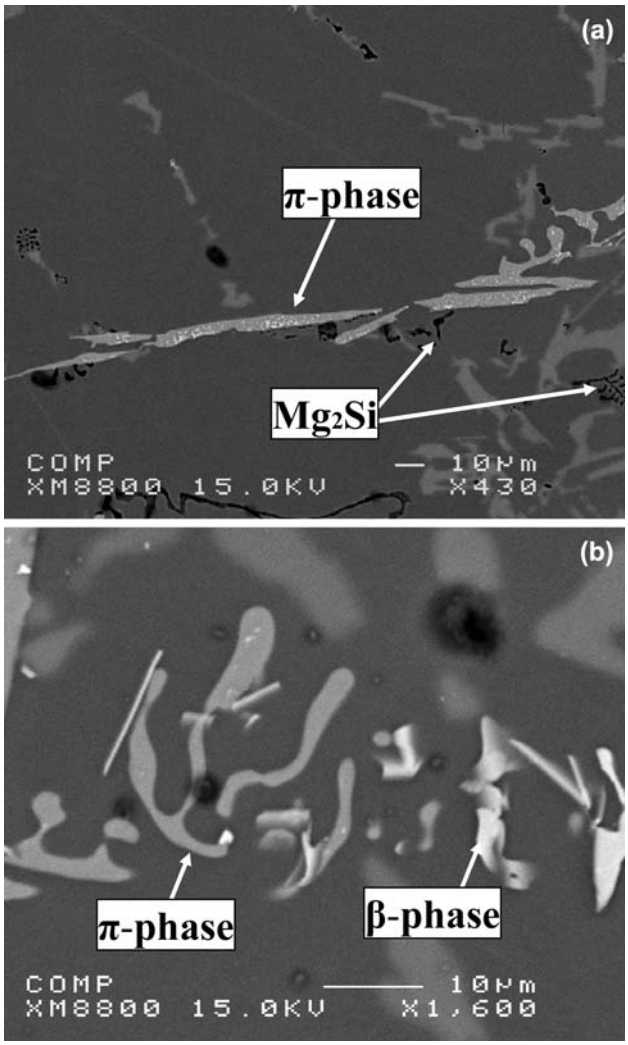

Fig. 8 Backscattered electron images of non-modified 357 alloy coded 11 in the **a** as-cast condition, showing π-phase, and **b** after solution heat treatment (540 °C/8 h) showing partial decomposition of π-phase into fine β-phase needles

These spheroidized particles are expected to be in the process of decomposition into β-phase needles. The X-ray images showing the distribution of Fe and Mg in the decomposed β-phase (Fig. 7c, d) confirm this observation. Based on the latter, it may be suggested that the incomplete decomposition of the π-phase into β-phase needles in solution heat-treated Sr-modified Al–7Si–0.4Mg–0.1Fe alloys is most likely related to the existence of large π-phase particles for which a greater solution heat treatment time is required to complete the decomposition process.

It may also be observed from Fig. 5a and b that when the Mg content is >0.4 wt% in Al–7Si–*x*Mg–*y*Fe alloys, there is an increase in the resistance of the π-phase to completely decompose into β-phase during solution heat treatment in both the non-modified and the Sr-modified alloys when compared to low Mg (0.4 wt%) alloys. This observation may be supported by the microstructures of the solution heat-treated non-modified Al–7Si–0.75Mg–0.1Fe alloy, shown in Fig. 8. While Fig. 8a corresponds to the as-cast microstructure, Fig. 8b shows small amounts of π-phase particles decomposed into fine β-phase needles while the remaining amount displays fragmentation and spheroidization after solution heat treatment. The chemical composition of the π-phase as obtained by EPMA and WDS in the Al–7Si–0.8Mg–0.1Fe alloy in the as-cast and solution heat-treated conditions, is listed in Table 6, reveals that there is almost no change in the composition of π-phase in both the conditions. It can be seen that the calculated stoichiometry of the π-phase in both the conditions approaches the suggested formula of $Al_8FeMg_3Si_6$.

It has been reported that the maximum solubility of Mg in Al–7Si–Mg alloys at 540 °C is ~0.6-wt% Mg [20]. Accordingly, and based on the observations of the π-phase decomposition in Al–7Si–*x*Mg–0.1Fe alloys, it may be suggested that the π-phase occurring in alloys containing less than 0.6-wt% Mg is expected to decompose to a large extent into β-phase needles after solution heat treatment. The extent of the decomposition would depend on how far the removed Mg content of the alloy is from the solubility limit at 0.6 wt%. At Mg contents >0.6 wt%, the π-phase is likely to undergo only partial decomposition into β-phase needles.

Table 6 Chemical composition of the **π**-phase formed in Al–7Si-0.6Mg–0.1Fe alloy before and after solution heat treatment

Alloy	Phase	Element				Formula	
		Al	Si	Fe	Mg	Calculated	Suggested [6, 22]
7Si–0.8Mg–0.1Fe as-cast	π	48.3	27.0	5.88	18.57	$Al_{7.8}Fe_{0.95}Mg_3Si_{4.4}$	$Al_8FeMg_3Si_6$
7Si–0.8Mg–0.1Fe solution heat-treated (540 °C/8 h)	π	48.4	26.7	5.33	18.5	$Al_{7.8}Fe_{0.86}Mg_3Si_{4.3}$	$Al_8FeMg_3Si_6$

Effects of beryllium addition

With regards to the purposes of this study, it was observed that the addition of 500-ppm Be in the as-cast Al–Si–*x*Mg–0.1Fe alloy containing 0.4, 0.6, and 1.0-wt% Mg has the potential for decreasing the amount of the surface fraction of π-phase intermetallic in both non-modified and Sr-modified alloys, as shown in Fig. 9a and b, respectively. This reduction may be ascribed to two factors: (1) the effect of Be addition on Al–7Si–Mg alloys in transforming the β-phase into a Chinese-script α-AlFeSi iron intermetallic phase (Fig. 10) having a stoichiometry of $Al_{6.9}Fe_2Si_{1.4}$ which is close to A_8Fe_2Si, as found in the literature [31], and (2) the formation of Be–Fe phases with script morphology in Be-containing Al–7Si–0.6Mg alloys (Fig. 11), which form at higher temperatures than those of the β-phase, thereby reducing the Fe available to form β- and π-phases [16, 32].

A decrease in the π-phase surface fraction with respect to an increase in Mg from 0.4 to 1.0 wt% was observed after solution heat treatment in the non-modified and the Sr-modified Be-containing Al–7Si–*x*Mg–0.1Fe alloys, as shown in Fig. 9a and b, respectively. At 0.4-wt% Mg and after solution heat treatment, the π-phase is observed to have completely decomposed in both the non-modified and the Sr-modified Be-containing alloys, while at 0.6-wt% Mg, the π-phase is seen to have only partially dissolved. This observation is supported by the Be-containing Al–7Si–0.6Mg–0.1Fe alloy microstructure (Fig. 12). Figure 12a shows the π-phase in the as-cast condition, while Fig. 12b reveals that the π-phase has partially decomposed into small β-phase particles.

In order to acquire a clearer understanding of the role of Be in conjunction with a high amount of Mg, the Mg content in the Al–7Si–*x*Mg–0.1Fe alloy was increased to 1.0 wt%. Figure 13a shows the microstructure of the

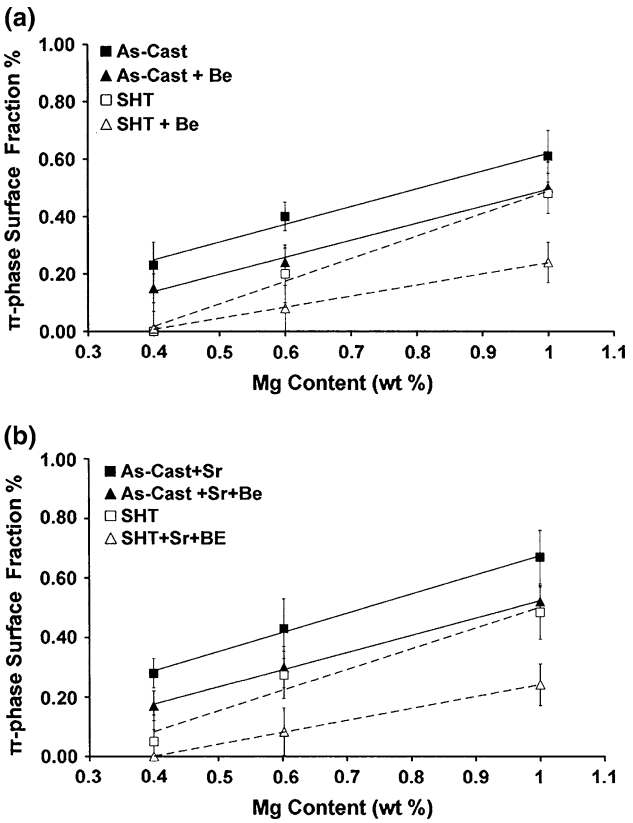

Fig. 9 Effects of solution heat treatment (540 °C/8 h) on the surface fraction of the π-phase in Al–7Si–*x*Mg–0.1Fe Be-containing alloys **a** non-modified alloys and **b** Sr-modified alloys

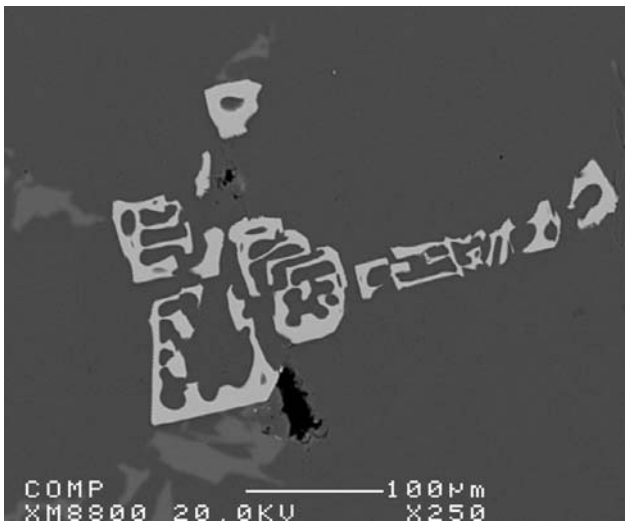

Fig. 10 Backscattered electron images of Be-containing 357 alloy 6B in the as-cast condition (DAS = 110 µm), showing the α-Al_8Fe_2Si iron intermetallic phase

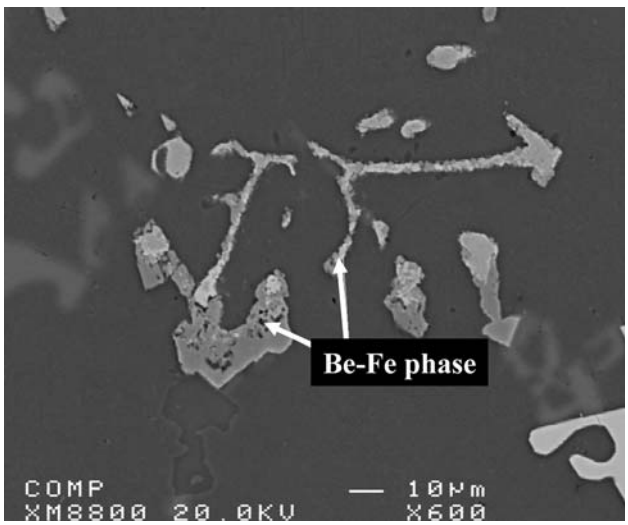

Fig. 11 Backscattered electron images of Be-containing 357 alloy 6BS in the as-cast condition (DAS = 110 µm), showing the Be–Fe phase

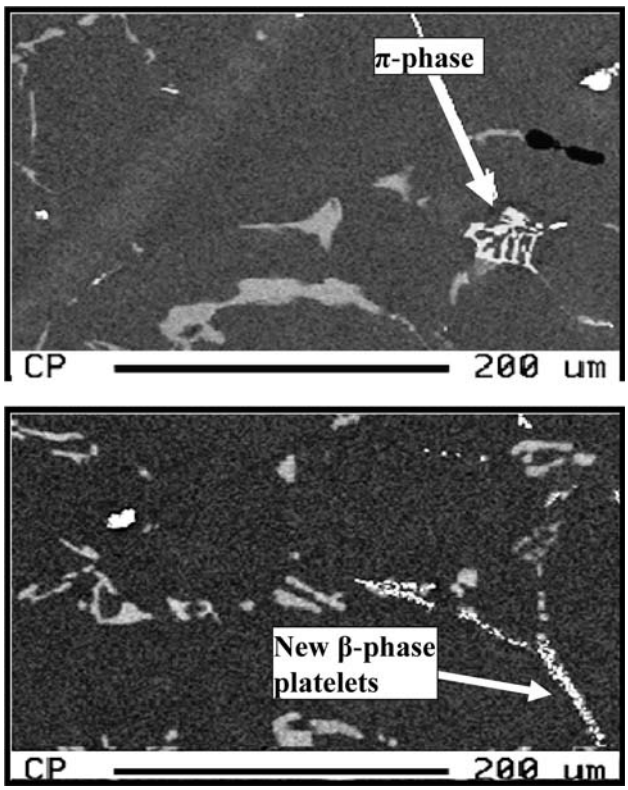

Fig. 12 Backscattered electron images of Be-containing 357 alloy 6B in the **a** as-cast condition, showing the π-phase intermetallic and **b** after solution heat treatment (540 °C/8 h), showing the decomposition of π-phase into β-phase particles

as-cast Be-free Al–7Si–1.0Mg–0.1Fe alloy, while Fig. 13b shows a large π-phase particle (on the right) and small fragments of the π-phase (on the left) in a microstructure of the same alloy after solution heat treatment. The X-ray image in Fig. 13c shows the distribution of Mg, confirming this to be the π-phase. On the other hand, the addition of 500-ppm Be to the same Al–7Si–1.0Mg–0.1Fe alloy results in the existence of small bright particles around the π-phase after solution heat treatment, as shown in the back-scattered electron image of Fig. 14a. Figure 14b, c, and d depicts the X-ray images corresponding to the distributions of Mg, Si, and Fe, respectively, in the decomposed π-phase, in supporting the assertion that the bright particles around the π-phase are β-phase particles.

According to this observation, it may be suggested that the addition of Be in amounts of 500 ppm to Al–7Si–xMg–0.1Fe alloys results in reducing the size and amount of π-phase which facilitates the decomposition process of the π-phase into β-phase particles during solution heat treatment, especially at high Mg levels when compared to Be-free alloys. Based on an examination of the microstructure, it becomes apparent that the decomposition mechanism of the π-phase into β-phase during solution

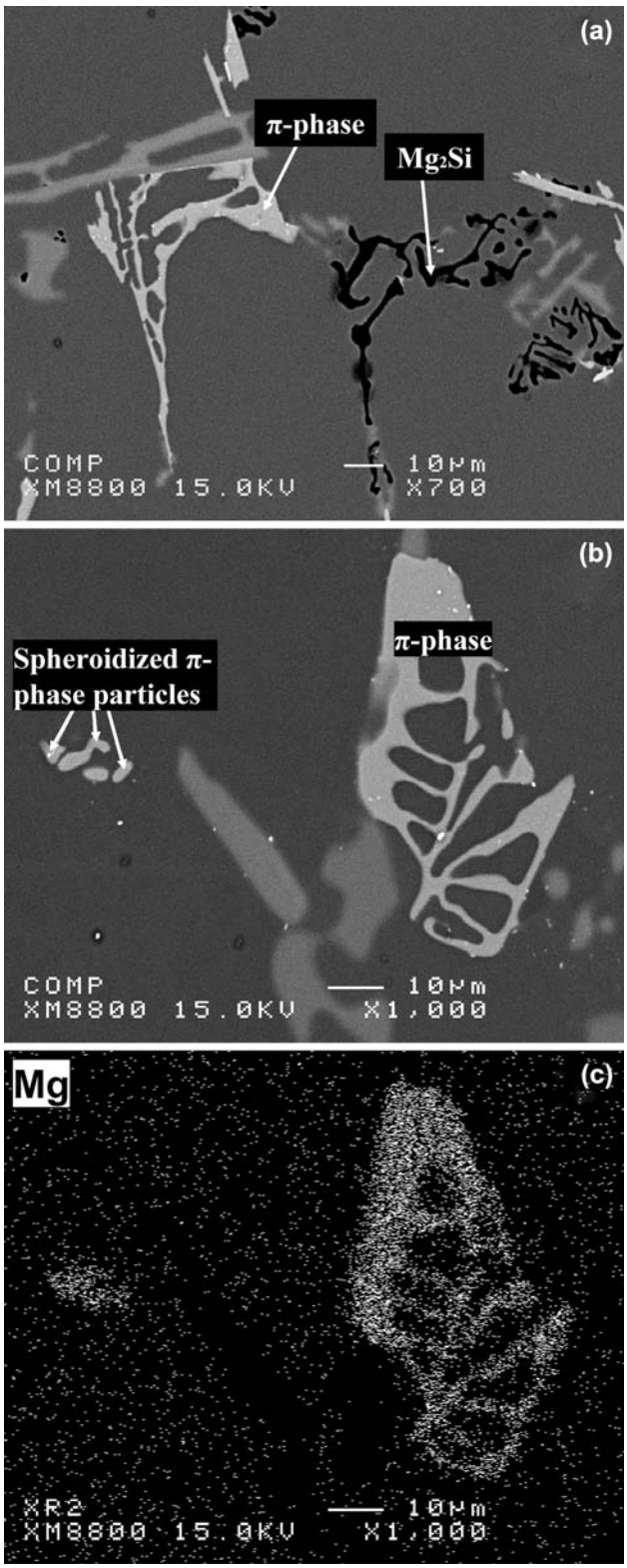

Fig. 13 Backscattered electron images of Be-free Al–7Si–1.0Mg–0.1Fe alloy 16 in the **a** as-cast condition, showing the π- and β-phases, **b** after solution heat treatment (540 °C/8 h), showing the fragmentation of the π-$Al_8Mg_3FeSi_5$ phase, **c** X-ray image of Mg corresponding to (**b**)

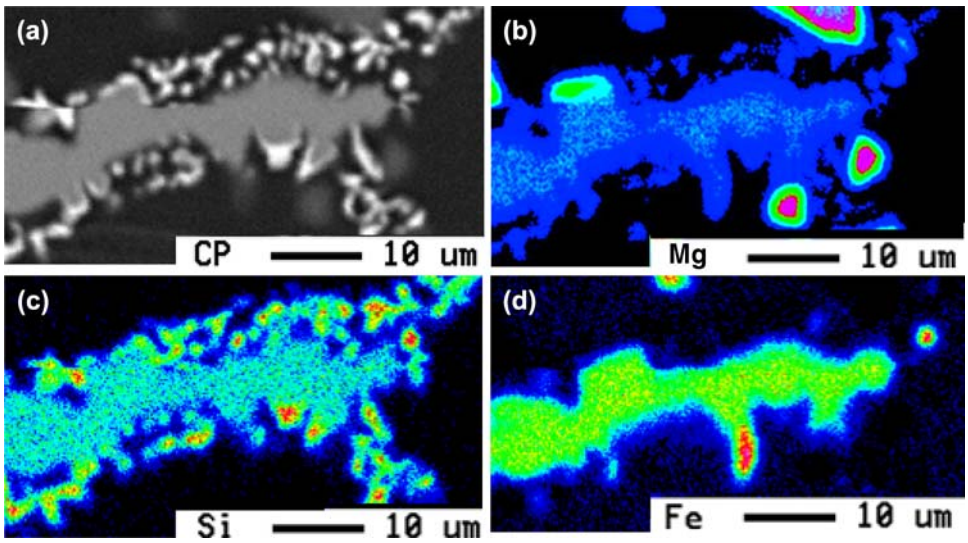

Fig. 14 **a** Backscattered electron image obtained from Be-containing Al–7Si–1.0Mg–0.1Fe alloy 16B after solution heat treatment (540 °C/8 h), showing the decomposed π-phase and corresponding X-ray images of Mg (**b**), Si (**c**), and Fe (**d**) in the same

heat treatment is expected to occur as such during solution heat treatment, the Al, Si, and Mg must diffuse out from the π-phase into the aluminum matrix, forming a layer of β-phase particles around the π-phase; as the diffusion of the elements proceeds over time, the π-phase is expected to display more decomposition. In order to fully obtain the detailed mechanism by which the π-phase decomposed into the β-phase during solution heat treatment, further experimental study, such as quantitative and qualitative evaluations of the π-phase decomposition process at different solution heat treatment times, as well as an investigation into the impact of this decomposition on the chemistry of the Al-matrix, is required.

Conclusions

From an analysis of the results, the following may be concluded:

1. Analysis of the Al–7Si alloys with varying amounts (wt%) of Mg and Fe indicates that the amount of the π-phase increases as the percentage weight of both the elements increase.
2. Addition of Sr leads to slight increases in the π-phase surface fraction in Al–7Si–*x*Mg–*y*Fe alloys.
3. Solution heat treatment leads to a significant reduction in the surface fraction of the π-phase in all alloys studied.
4. After solution heat treatment, the Chinese-script π-phase is completely decomposed into fine needles of β-phase at 0.4-wt% Mg, but appears to be only partially decomposed at higher Mg contents (0.4–0.8 wt%).
5. According to the qualitative and quantitative analyses, the optimum Mg levels at which the π-phase shows a high degree of decomposition into β-phase after a solution heat treatment of 540 °C/8 h is in the range of 0.4–0.6-wt% Mg.
6. The addition of 500-ppm Be reduces the amount of the π-phase formed in Al–7Si–*x*Mg–0.1Fe. Such additions also facilitate the decomposition of the π-phase into β-phase, particularly at higher levels of Mg content (1.0 wt%).

Acknowledgements The authors would like to express their grateful acknowledgment for financial support received from the Natural Sciences and Engineering Research Council of Canada (NSERC) and from Alcoa Canada Ltd. A part of the research presented in this paper was financed by the Fonds Québécois de la Recherche sur la Nature et les Technologies (FQRNT) through the intermediary of the Aluminum Research Centre – REGAL.

References

1. Hatch JE (1984) Aluminum: properties and physical metallurgy. ASM, Metals Park, p 50
2. Malgorzata W (2004) Aluminum-silicon casting alloys: an atlas of microfractographs, vol 124. ASM International Publisher, Materials Park, OH
3. Gilbert J, Leroy E (2004) Aluminum alloy castings: properties, processes and applications. AFS, ASM International, Materials Park
4. Murali S, Raman KS, Murthy KSS (1992) Mater Sci Eng A151:1
5. Vorren O, Evensen JE, Pedersen TB (1984) AFS Trans 92:459
6. Bäckerud SL, Chai G, Tamminen J (1990) Solidification characteristics of aluminum alloys. Oslo, Norway
7. Cáceres CH, Davidson CJ, Griffiths JR, Wang QG (1999) Met Trans A 30A:1999
8. Wang QG (2003) Met Trans A 34A:2887
9. Joenoes AT, Gruzleski JE (1991) Cast Metals 4:6271

10. Thirugnanam A, Sukumaran K, Pillai UTS, Raghukandan K (2007) Mater Sci Eng 445–446:405
11. Barresi J, Kerr MJ, Wang H, Couper MJ (2000) AFS Trans 108:563
12. Wang QG, Cáceres CH (1997) Mater Sci Forum 242:159
13. Wang QG, Davidson CJ (2001) J Mater Sci 36:739. doi:10.1023/A:1004801327556
14. Granger A, Sawtell RR (1984) AFS Trans 92:579
15. Wikle KG (1978) AFS Trans 86:513
16. Tan YH, Lee SL, Lin Y (1995) Met Trans A 26A:1195
17. Murali S, Raman KS, Murthy KSS (1994) Cast Metals 6:189
18. Murali S, Raman KS, Murthy KSS (1995) Mater Sci Eng A190:165
19. Zalensas DL (2001) Aluminum casting technology, 2nd edn. AFS, Des Plaines, p 19
20. Apelian D, Shivkumar S, Sigworth G (1989) AFS Trans 97:727
21. Shivkumar S, Keller C, Trazzera M, Apelian D (1990) Precipitation hardening in 356 alloys. In: Proceedings of the international symposium on production, refining, fabrication and recycling of light metals, Hamilton, Ontario, pp 264–278
22. Closset BM, Gruzleski JE (1982) Met Trans A 13A:945
23. Gustafsson G, Thorvaldsson T, Dunlop GL (1986) Met Trans A 17A:45
24. Taylor JA, StJohn DH, Barresi J, Couper MJ (2000) Mater Sci Forum 331–337:277
25. Gruzleski JE, Closset BM (1990) The treatment of liquid aluminum-silicon alloys. AFS, Inc, Des Plaines
26. Foss S, Olsen A, Simensen CJ, Tafto J (2003) Acta Crystall B59:36
27. Lu L, Dahle AK (2005) Met Trans A 36:819
28. Lu L, Dahle AK, Couper MJ (2004) Solidification of aluminum alloys. TMS, Warrendale
29. Moustafa MA, Samuel FH, Doty HW, Valtierra S (2003) Int J Cast Metals Res 15:609
30. Samuel FH, Ouellette P, Samuel AM, Doty HW (1998) Met Trans A 29A:2871
31. Yang CY, Lee SL, Lee CK, Lin JC (2005) Mater Chem Phys 93:412
32. Sreeja Kumari SS, Pillai RM, Rajan TPD, Pai BC (2007) Mater Sci Eng 460–461:561